

# SPG MITTEILUNGEN

# COMMUNICATIONS DE LA SSP

## AUSZUG - EXTRAIT

### Progress in Physics (61)

**Two-post wave slaloming at a cut-off and a resonance, or how to access and heat “overdense” plasmas using two successive mode conversions**

*Antoine Pochelon<sup>1</sup>, Loïc Curchod<sup>1</sup>, Prabal Chattopadhyay<sup>2</sup>, Duccio Testa<sup>1</sup> and the TCV team  
<sup>1</sup> EPFL, Swiss Plasma Center, Lausanne, Switzerland; <sup>2</sup> IPR, Bhat, Gujarat, India*

This article has been downloaded from:

[https://www.sps.ch/fileadmin/articles-pdf/2018/Mitteilungen\\_Progress\\_61.pdf](https://www.sps.ch/fileadmin/articles-pdf/2018/Mitteilungen_Progress_61.pdf)

© see [https://www.sps.ch/bottom\\_menu/impressum/](https://www.sps.ch/bottom_menu/impressum/)

## Progress in Physics (61)

### Two-post wave slaloming at a cut-off and a resonance, or how to access and heat “overdense” plasmas using two successive mode conversions

Antoine Pochelon <sup>1</sup>, Loïc Curchod <sup>1</sup>, Prabal Chattopadhyay <sup>2</sup>, Duccio Testa <sup>1</sup> and the TCV team  
<sup>1</sup> EPFL, Swiss Plasma Center, Lausanne, Switzerland; <sup>2</sup> IPR, Bhat, Gujarat, India

Two mountaineering analogies illustrate well the content of this article on electron cyclotron resonance heating (ECRH) in tokamaks. When skiing, you can either go straight down the slope or practise some slaloming. The article first describes “straight” trajectories as in ECRH basic schemes, then what slaloming skills can add.

And the second analogy, when hiking you know perfectly well that you cannot pass anywhere, that there are trails that lead you to passes, where free progression is easy, or to steep faces where progression is blocked. Something very similar happens for electromagnetic waves propagating in inhomogeneous plasmas with density and magnetic field gradients. This makes some places inaccessible.

For example, the blackout when re-entering the atmosphere. An astronaut knows that he will be in radio blackout for a while due to the friction of the vehicle against the atmosphere forming an ionized gas shield. The electromagnetic waves are reflected in the plasma density gradient at the location of the plasma electrostatic resonance frequency  $\omega_p = (\eta_e e^2 / m_e \epsilon_0)^{1/2}$ , which, in the absence of magnetic field determines the only cut-off (with  $n_e$ ,  $e$ ,  $m_e$ , the electron density, charge, mass, and  $\epsilon_0$  the vacuum dielectric constant) [1,2].

#### EC heating scheme (“straight” propagation)

In the torus-shaped plasma of a tokamak we have both a radially inhomogeneous density (along the small radius  $a$ ) and magnetic field  $B \sim 1/R$ , where  $R$  is the big radius. The waves are absorbed where their frequency, or harmonics, match the electron cyclotron resonance  $\omega_{ce} = eB/m_e$ , a vertical line in Fig.1. The presence of a magnetic field determines the two polarizations of the e-m wave, with two additional cut-offs. The usage defines the waves with the oscillating electric field *parallel* to the static magnetic field  $B$  as the “ordinary” wave, or O-mode of propagation, and when *perpendicular*, the “extraordinary” wave, or X-mode of propagation. The microwave sources used to heat plasmas are typically in the 50 - 200 GHz ranges, where 500 kW - 2 MW continuous-wave (CW) gyrotrons are developed [3].

In the standard tokamak situation, comfortable technical access to the centrally located vertical EC resonance for microwave launchers is provided from the outside, i.e. from the low magnetic field side of the tokamak (LFS). From that place, typically 100% absorption of the X-mode is afforded at the “second harmonic” X2,  $2\omega_{ce}$ , and good absorption at the 3<sup>rd</sup> harmonic, X3, at sufficiently high plasma electron temperature, Fig. 1. This makes ECRH an operationally excellent heating with localized power deposition property, providing like a surgical tool for heat-transport studies or for the control of temperature-profile-dependent plasma in-

stabilities. The propagation from the plasma edge is nearly straight at low densities, allowing access to the (X2, X3, O1)-resonances but stopped at high-density by refraction in “overdense” plasmas, that is by plasma above cut-off density. Let us further mention that fundamental X-mode launch from the LFS is blocked very close to plasma edge by the “right-hand” polarisation cut-off (“R” in Fig. 4). Fundamental O-mode resonance heating is suitable for high-field machines like ITER ( $\sim 5$  Tesla) but limited due to insufficient absorption at 2<sup>nd</sup> or 3<sup>rd</sup> harmonic (O2, O3).

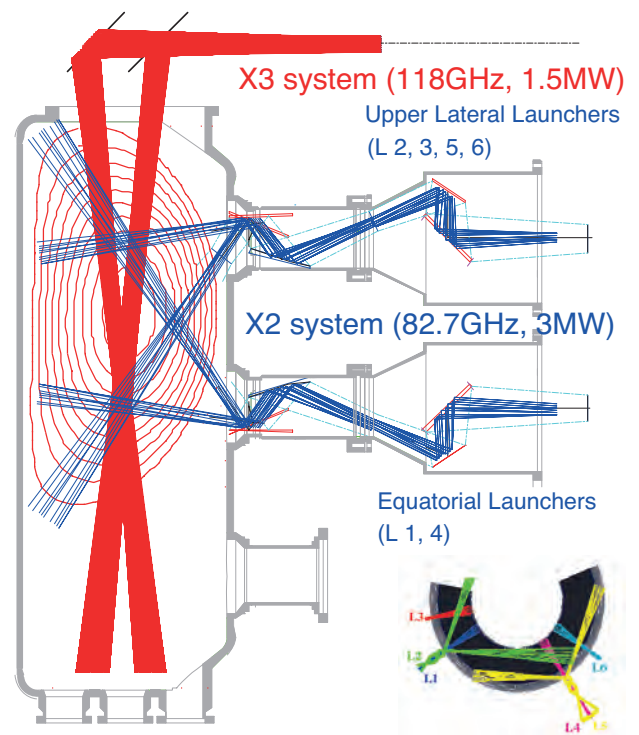


Fig. 1: Electron cyclotron resonance heating at the 2<sup>nd</sup> (X2) and 3<sup>rd</sup> harmonic (X3) in the TCV tokamak (Tokamak à Configuration Variable). Tokamak axis on the left, LFS on the right.

#### Electron Bernstein Wave heating (2 post slaloming)

There is a class of low-field tokamak, however, where the easy “straight” propagation of (X2, X3) is insufficient to access the full high-density range these machines can produce, as developed in Box 1. These devices include low aspect ratio ( $R/a \sim 1.3$ ) “spherical tokamaks” (0.2 - 2 T), like the MAST tokamak (0.5 T) [7], Fig. 3, or the T-15 device (2 T) [8] and stellarators [9].

Luckily, nature provides us with a slaloming trick to reach overdense plasma cores: the microwave beam is launched in O-mode polarisation, thwarting the X-mode cut-off at the plasma edge, and soon after having crossed this edge-cut-off, the O-wave changes its identity to X-mode. It nearly resembles a fairy tale, plasma version!

### Waves versus machines high-density limits in ECRH ("straight" propagation)

It is clearly optimal to choose a heating method covering at best the operational density range of a given device. We compare therefore the limitation due to EC cut-offs with the specific tokamak plasma density limit, described by the empirical Greenwald density limit  $\langle n_{eG} \rangle = 0.27 I_p / a^2$  [4], thus grossly proportional to  $B/R$  (plasma current  $I_p$ , big and small tokamak radius  $R$  and  $a$ ).

The accessibility of EC waves depends primarily on the machine magnetic field, which determines the cut-off densities and cyclotron resonance location. The typical nominal magnetic field in tokamaks extends from the low field spherical tokamaks  $B \sim 0.5$  T, through the medium field TCV  $B = 1.5$  T, to the high field ITER machine 5.3 T.

The adequation of the EC wave scenario can be expressed by the ratio of EC cut-offs density versus machine accessible density range,  $n_{e\_cutoff} / n_{eOG}$  given in % in Fig.2 [5]. The field is sufficiently high in ITER to allow access to the complete machine density range using the fundamental O1 at 170 GHz. In low-field machines however, like the spherical tokamaks, the lowest harmonics ECWs give only access to a few percentages of  $n_{eG}$ . In the medium field TCV machine, 10% of  $n_{eG}$  is accessible with X2, a range extended to 26% with X3, leaving a large density range uncovered.

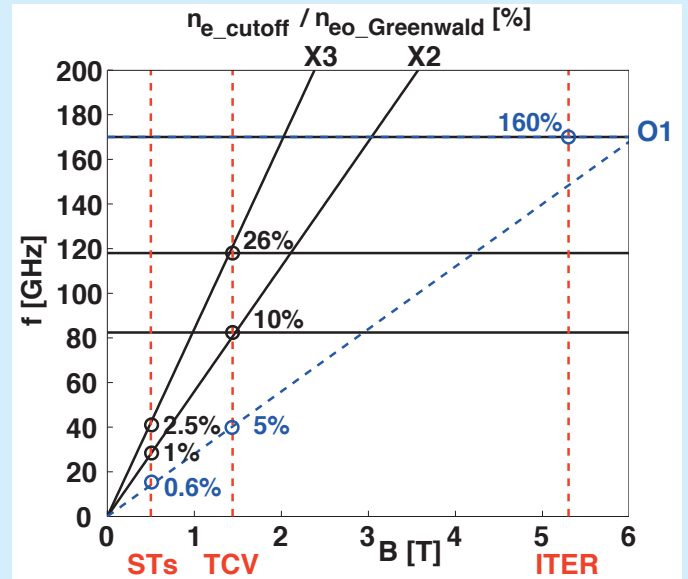


Fig. 2: Ratio of EC wave maximum density limit (cut-off density) to tokamak density limit (Greenwald limit) for different gyrotron frequencies and nominal tokamak magnetic fields given in %, for the O1-, X2- and X3-heating scheme, representing the "density coverage" of a given ECRH, optimally wished to be 100% (from [5]).

A more general and recommended description of resonances and cut-offs is provided by the CMA-diagram (Clemmow-Mullaly-Allis), that gives a compact representation of the solutions of the dispersion relation of electromagnetic waves in inhomogeneous density and magnetic field plasmas [1,2,6].

But a bit more physically, to achieve this, the identity change to X-mode polarisation is obtained through reflection at the O-mode cut-off. Fishermen, wearing polarising glasses to exclude the light polarised by reflection at the air-water interface are in fact using the same property, which allows them to see the fishes below the surface. This reflection at the O-mode cut-off represents our first slalom post.

At a proper incidence angle of around  $40^\circ$  from the normal to the magnetic field, the quasi-totality of the O-wave is converted to the X-wave [10], which then bounces back towards the plasma edge until it reaches the upper-hybrid electrostatic resonance (UHR), where the wave becomes stagnant, accumulating electric field. This represents our second slalom post.

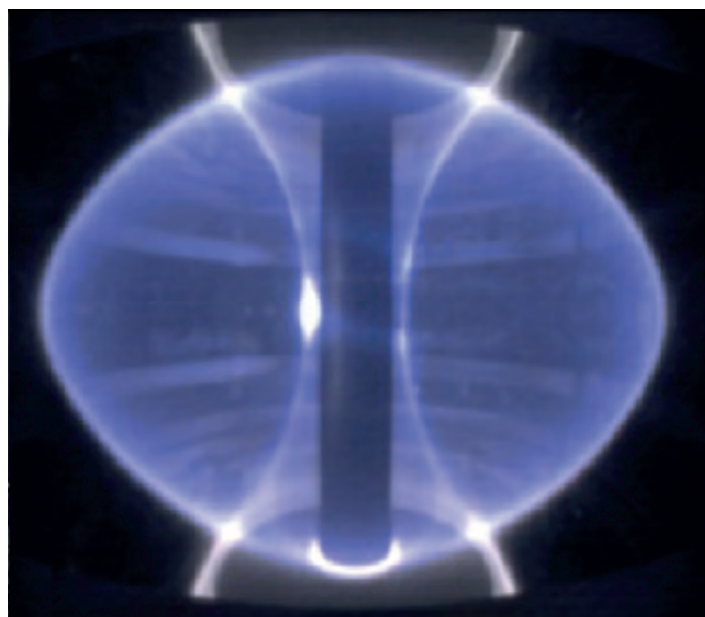


Fig. 3: The "spherical" tokamak plasma in MAST, Culham, UK, an example of low B-field, low aspect ratio tokamak. © CCFE.

Here at the UHR, the X-mode is known to convert to both 1) an electron Bernstein wave (EBW or "B"), an electrostatic mode propagating to the plasma core with no density limitation and dissipating in the region of the EC resonance or its harmonics [11], and to 2) parametrically driven lower-hybrid waves (Lower Hybrid Parametric Instability, LHPI) [9,12]. The full wave path of the  $O \rightarrow X \rightarrow B$  wave conversion is schematically depicted in Fig. 4.

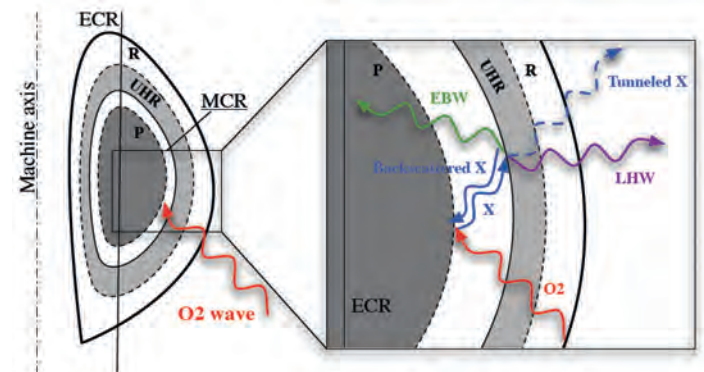


Fig. 4: Wave conversion processes following O2 injection in overdense plasma:  $O2 \rightarrow X \rightarrow B + LH + losses$ . Courtesy [13].

That such an O-X-B wave conversion scheme was potentially attractive for overdense plasma heating was in fact perceived early by the Electron Cyclotron Resonance Ion Sources (ECRIS) community, since these sources were amazingly capable of working efficiently above cut-off density [6,14]. ECRIS are used in various fields like particle beams, metal ion beams, accelerators or cancer therapy. The use of the O-X-B scheme to heat toroidal fusion plasmas started later in devices with high-density limits, like stellarators [9], or low field tokamaks, where high density “overdense” plasmas are only accessible by this scheme.

### Electron Bernstein Wave Heating using power modulation

The flexibility in plasma shape of the medium aspect ratio TCV tokamak and EC heating system was used to study the principle of the O-X-B heating scheme at high power (EBW).

The optimal injection angle of the second harmonic O-mode (O2) was first estimated with ray tracing simulation including O-X-B double mode conversion [15]. Around the calculated angle obtained, experimental launcher angle scans were performed to maximize plasma absorption by minimizing stray radiations. The experimentally determined optimum angles showed a good overlap with the ray tracing code results, a strong indication that O-X-B mode conversion was at work [16].

Power modulation experiments at 0.5 MW level were then performed at the experimentally determined optimal angle. The overall absorbed power was determined with a diamagnetic probe, that measures the toroidal magnetic flux variation directly related to the plasma stored energy. It shows the absorption of typically 60% of the incoming O2-mode waves, whereas for X2-mode injection, the absorption was vanishingly low (below 10%). This is a further strong indication that O2-mode waves must therefore mode convert and make their way further into the plasma, while X2-injected waves are reflected back (R cut-off, Fig.4), as expected for overdense plasmas.

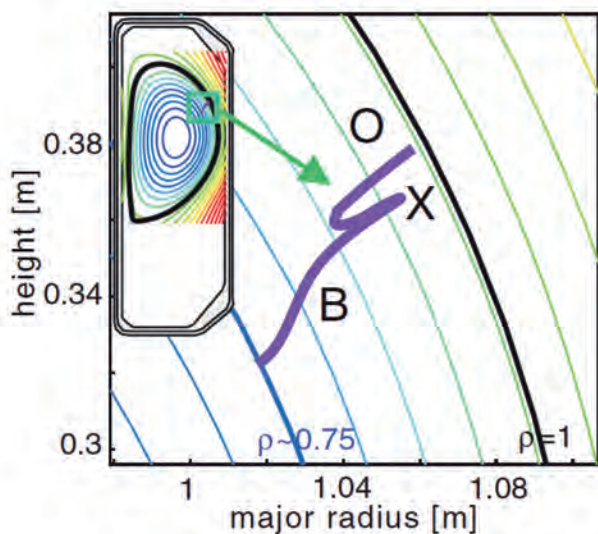


Fig. 5: Poloidal projection of the calculated O2 ray trajectory launched from the LFS, with its successive conversions to X-mode and to Bernstein waves (B).  $\rho$  is the normalized radius with  $\rho = 1$  representing the plasma edge,  $\rho = 0.75$  the absorption location [16].

The next step in the demonstration of EBW absorption is checking the power deposition location. Slightly off-axis power deposition location, but still well inside the plasma cut-off, was selected, as shown in Fig. 5, to avoid the perturbing effect of naturally occurring central relaxations. The deposition location was determined experimentally using the soft X-ray emission measured by a multi-wire proportional detector (Charpak detector) with vertical line-of-sights and viewing the plasma through 100  $\mu\text{m}$  beryllium-window thickness [17], as shown in Fig. 6.

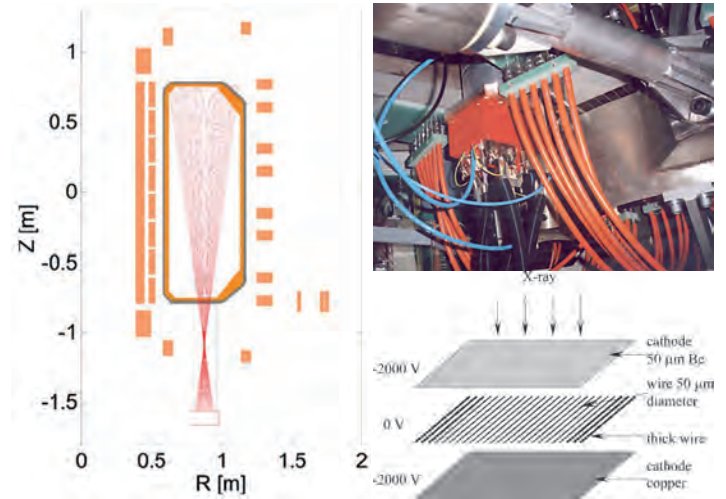


Fig. 6: The 64-channel soft X-ray Charpak-chamber camera for the detection of heat deposition location.

The local heat deposition caused by the modulated EC power is visible in the line-integrated time traces of several channels, on both the HFS (high field side) and the LFS. The deposition location is first evaluated using fast Fourier transform (FFT) analysis of the 64 soft X-ray chord signals. The FFT amplitude at the power modulation frequency is plotted against the soft X-ray channel number in Fig. 7(a), showing two clear amplitude maxima. These broad spatial maxima correspond to emission at the normalized radius  $\rho \sim 0.65$ , on both the HFS and the LFS. The maximum on the HFS is more pronounced, due only to line integration effects.

To remove the effect of line-integration, the profile is tomographically inverted. Fig. 7(b) plots the FFT amplitude of the inverted data at the power modulation frequency against the normalized radius  $\rho$ . The radial maximum of the FFT amplitude, after inversion, is located at  $\rho \sim 0.71$ , well inside the plasma cut-off and close to the location calculated by ray tracing, at  $\rho \sim 0.78$ , i.e. within 10% of the radial coordinate.

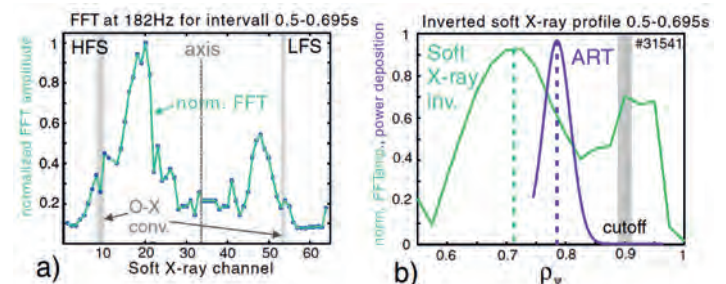


Fig. 7: Detection of the power deposition location by the power modulation technique using the 64-channel soft X-ray camera a) Normalised FFT amplitude of the line-integrated soft X-ray at the modulation frequency, b) Tomographic inversion yielding the radial deposition location [16].

The slight difference may be attributed to uncertainties in the magnetic equilibrium reconstruction and the density gradient measurement. The edge soft X-ray signals indicate a further stray power deposition just outside the cut-off, possibly resulting from 2<sup>nd</sup> harmonic X-mode absorption of non-O-X-B-converted wave power absorbed after multiple wall reflections and mode scrambling.

The good agreement between the simulated and experimental radial deposition locations, together with deposition at an overdense location, constitutes again strong proof that the O-X-B conversion mechanism is at work.

### Long-pulse high-power EBW Heating

To demonstrate heating with a substantial central temperature increase due to EBH, the pulse duration was extended to 100 ms, longer than the energy confinement time ( $\tau_E \sim 50$  ms), and the total power was increased to 2 MW with a modulation depth of 1 MW, as shown in Fig. 8. The injection angles of the four launchers used were chosen so as to heat with all of them at the same "overdense" location at  $\rho \sim 0.4$ , where  $(\omega_{pe}/\omega)^2 \sim 1.5$ . The more central deposition was achieved by lowering the machine magnetic field to bring the 2<sup>nd</sup> harmonic resonance further to the HFS [18].

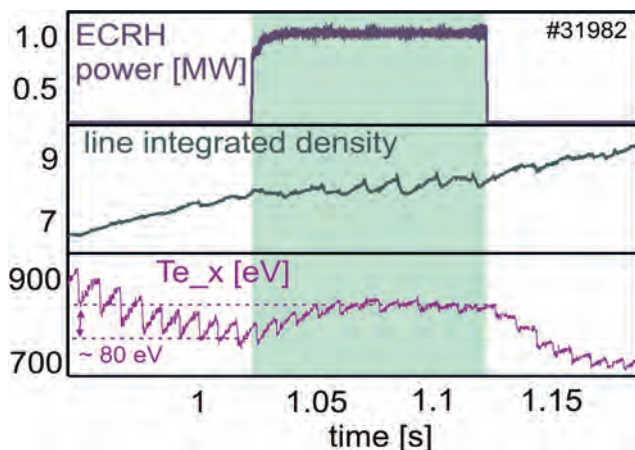


Fig. 8: Long pulse 1 MW EBH heating, 100 ms, on top of a longer 1 MW (not shown), demonstrating electron temperature increase due to EBWH [18].

The central electron temperature evolution is measured by the "absorber method", using a few soft X-ray diodes equipped with different beryllium thicknesses aiming at the plasma core. This showed a consistent increase in central electron temperature of  $T_e \sim 80$  eV during the EBH pulse, Fig. 8. This increase is confirmed by the Thomson scattering measurements. With the total injected power of 2 MW, large edge instabilities were developing at a slow repetition rate (16 ms), stabilizing the plasma density and thus ensuring that the temperature increase is directly attributable to EBW heating. These experiments represent the first demonstration of EBW heating in a medium aspect ratio tokamak at high power [16].

### Parasitic losses at the second slalom post?

These successful heating results imply that a large fraction of the power launched is converted to Bernstein waves. It is now important to address the issue of the efficiency of the whole wave conversion process. The diamagnetic probe found 60% of power absorbed in the plasma. This is raising the issue of possible non-converted power or power chan-

nelled to unknown paths. What really happens at the UHR, how much power is channelled to the B waves and to the "parasitic" LH waves, what is the power dependence and the role of the non-linear effects prone to occur at the UHR, defines the next studies.

To experimentally better identify the conversion processes at the UH-layer, a loop-probe has been designed and inserted in TCV scrape-off layer outside the confined plasma, with a flat response to e-m. waves over the LH-waves frequency range to study (0.2 - 10 GHz) [13]. As the injected power is increased, the whole spectrum measured rises in amplitude and broadens towards higher frequencies as shown in Fig. 9. Despite the apparent complexity of these spectra, with new peaks systematically appearing as the power is raised, they are highly reproducible. But not straightforward to explain.

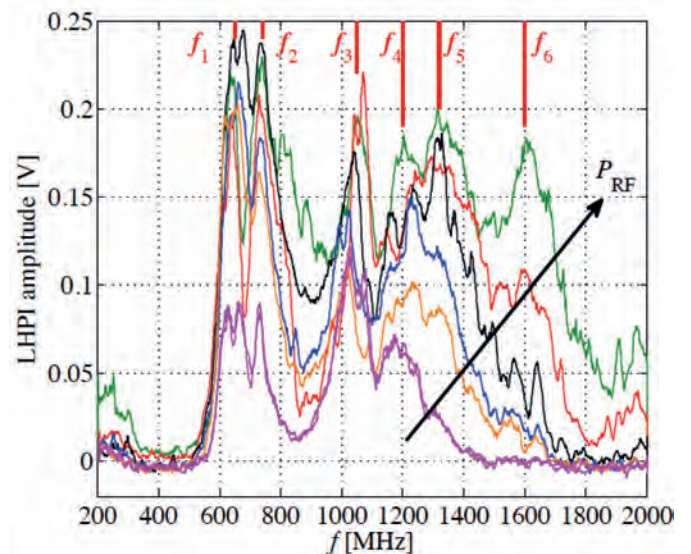


Fig. 9: Lower Hybrid Parametric Instability spectra broadening with increasing gradually injected O2 power from 30 to 530 kW [13].

Investigations of the nature of the wave conversion processes occurring in the O $\rightarrow$ X $\rightarrow$ B scheme have recently been undertaken using particle-in-cell (PIC) simulations [19]. These show new detailed results on the waves involved in these conversions, parametric effects and findings like the existence of an X-wave-instability. The large excited spectra found in these PIC simulations recall strongly the experimental LHPI-spectra measured in TCV. This is strongly suggesting that a thorough comparison of experiment and simulation would give further insight. It should also give helpful indications for the optimization of the power deposition and the evaluation of losses of the O-X-B heating scheme at high power.

The heating experiments described here represent a successful proof of EBW overdense heating at high power in a medium aspect ratio tokamak by using a double mode conversion process. To investigate the overall efficiency, the understanding of the wave channelling occurring at the UH resonance and its non-linear power dependence, is certainly a key element to maximize the conversion to Bernstein waves and to consolidate and validate this "overdense" heating scheme.

*This work was supported in part by the Swiss National Science Foundation.*

## References

- [1] T. H. Stix, 1992 *Waves in Plasmas* (New York: Springer).
- [2] A. Pochelon, *Electron Cyclotron heating* 1994 36<sup>th</sup> AVCP Course, LRP 505/94.
- [3] S. Alberti and T. M. Tran, *Electron Cyclotron Masers* 2014 SPG Mitteilungen 41, 28-30.
- [4] M. Greenwald et al., 1988 Nucl. Fusion **28** 2199.
- [5] A. Pochelon et al., *Recent physics results with electron cyclotron heating in TCV*, "Strong Microwaves in Plasmas", Nizhny Novgorod, **Vol. 2**, (2006) 421–433, Russian Acad. of Sciences, A. G. Litvak ed., ISBN 5-8048-0038-8.
- [6] R. Geller, *Electron Cyclotron Resonance Ion Sources and ECR Plasmas*, IoP Publishing 1996, ISBN 0-7503-0107-4.
- [7] A. Kirk et al., 2017 Nucl. Fus. **57**, 102007.
- [8] A. V. Melnikov, A. V. Sushkov et al., 2015 Fusion Engineering and Design **96–97** 306–310.
- [9] H. P. Laqua et al., 1997 Phys. Rev. Lett. **78** 3467.
- [10] E. Mjølhus 1984 J. Plasma Phys. **31** 7.
- [11] I. B. Bernstein 1958 Phys. Rev. **109** 10.
- [12] F. S. McDermott, G. Bekefi, K. E. Hackett, J. S. Levine and M. Porkolab, 1982 Phys. Fluids **25** 1488.
- [13] L. Curchod, *High-density plasma heating in the tokamak à Configuration variable*, Thèse EPFL 5012 (2011).
- [14] A. Pochelon, *Book review "ECRIS by R. Geller, IoP Publishing 1996" [6]*, 1997 Plasma Phys. and Contr. Fusion **39**, 6.
- [15] F. Volpe 2003 PhD Thesis Max-Planck Institut für Plasmaphysik, IPP Garching and Greifswald IPP Report 13/1.
- [16] A. Mueck, L. Curchod, et al., *Demonstration of Electron-Bernstein-Wave Heating in a Tokamak via O-X-B Double-Mode Conversion*, 2007 PRL **98**, 175004.
- [17] A. Sushkov et al., *High-resolution multi-wire proportional soft x-ray diagnostic measurements on TCV*, 2008 Rev. of Scientific Instruments **79**, 023506.
- [18] A. Pochelon, A. Mueck, L. Curchod, et al., *Electron Bernstein wave heating of over-dense H-mode plasmas in the TCV tokamak via O-X-B double mode conversion*, 2007 Nucl. Fusion **47** 1552–1558.
- [19] A. V. Arefiev, I. Y. Dodin, A. Köhn, E. J. Du Toit, E. Holzhauser, V. F. Shevchenko and R. G. L. Vann, *Kinetic simulations of X-B and O-X-B mode conversion and its deterioration at high input power*, 2017 Nucl. Fusion **57** 116024.